A multi-wavelength study of the compact M1 flare on October 22, 2002

G. Del Zanna
MSSL, University College London Holmbury St. Mary Dorking UK RH5 6NT

A. Berlicki
Observatoire de Paris, LESIA, F-92195 Meudon Principal Cedex, France

B. Schmieder
Observatoire de Paris, LESIA, F-92195 Meudon Principal Cedex, France
Institute of Theoretical Astrophysics, University of Oslo, Blindern, N-0315 Oslo, Norway

H.E. Mason
Department of Applied Mathematics and Theoretical Physics, University of Cambridge, Cambridge UK CB3 0WA

June 22, 2005

Abstract. In this paper we present a further study of the M1 class flare observed on October 22, 2002. We focus on the SOHO Coronal Diagnostic Spectrometer (CDS) spectral observations performed during a multi-wavelength campaign with TRACE and ground-based instruments (VTT, THEMIS). Strong blue-shifts are observed in the CDS coronal lines in flare kernels during the impulsive phase of this flare. From a careful wavelength calibration we deduce upflows of 140 km/s for the Fe XIX flare emission, with a pattern of progressively smaller flows at lower temperatures. Large line-widths were observed, especially for the Fe XIX line, which indicate the existence of turbulent velocities. The strong upflows correspond to full shifts of the line profiles. These flows are observed at the initial phase of the flare, and correspond to the "explosive evaporation". The regions of the blueshifted kernels, a few arc seconds away from the flare onset location, could be explained by the chain reaction of successive magnetic reconnections of growing emerging field line with higher and higher overlying field. This interpretation is evidenced by the analysis of the magnetic topology of the active region using a linear force-free-field extrapolation of THEMIS magnetograms.

Keywords: Sun: flare – Techniques: spectroscopic – Line: EUV

1. Introduction

The broadening and blue-shifting of spectral lines for high temperature emission during the initial phase of solar flares has been extensively studied in the X-ray wavelength range using data from SOLFLEX (cf. Doschek et al., 1979), the Solar Maximum Mission's (SMM's) X-ray polychromator (XRP) Bent Crystal Spectrometer (BCS) (cf Antonucci et al., 1982) and the BCS on YOHKOH (see, e.g., Bentley et al., 1994).

Plasma velocities deduced from Doppler-shift analyses were of the order of a few hundred km s^{-1}. This blueshifted emission was interpreted as evidence for chromospheric evaporation. However, these BCSs had no spatial resolution, so it was not possible to locate the source of the blueshifted X-ray emission. A further complexity in the interpretation of BCS spectra was due to the superposition (at different wavelengths) of stationary components originating from different locations. In general asymetric line profiles were observed, rather than totally shifted lines. Without spatial resolution in the BCS X-ray observations, any weak blue-shifted X-ray emission would swiftly be swamped by the strong stationary emission from the flare X-ray loops. In a recent paper, Warren and Doschek (2005) interpret these blue-shifted asymetries as a succession of independently heated threads within flare loop structures. To progress further, it is essential to spatially locate the high temperature blue shifted emission in relation to the flare loops and structures.

The SMM XRP Flat Crystal Spectrometer (FCS) had a limited spatial resolution ($14''$). Zarro et al. (1988) reported spatially confined Mg XI blue-shifted emission during the impulsive phase of a small flare. The Fe XXI line at 1354.1 Å emitted at about 10^7 K, was studied with the SMM Ultraviolet Spectrometer and Polarimeter (UVSP) instrument (with spatial resolution down to $3''$) . Mason et al. (1986) deduced upward flows in Fe XXI emitting plasma in excess of 200 km/s. Their observations supported the hypothesis of chromospheric evaporation in the footpoint region of what subsequently became soft X-ray emitting loops.

The Coronal Diagnostic Spectrometer (CDS) instrument on SOHO has the capability to simultaneously obtain spatial and spectral information for emission over a wide range of plasma temperatures. Using CDS, it is possible to locate the source of high temperature blue-shifted emission seen during a solar flare. Such observations are however rare. Czaykowska et al. (1999) reported SOHO/CDS observations of blueshifts in Fe XVI (3×10^6 K) and Fe XIX (8×10^6 K) lines. These observations were however performed more than one hour after the maximum of a two-ribbon M6.8 flare. The blue-shifts appeared to be located at the outer edges of the flare ribbons.

Spatially-resolved spectral information from CDS were reported by Del Zanna et al. (2002a) covering the entire evolution of a small flare. Long-lasting (over an hour) blue-shifts of 30 km/s in coronal lines (Mg X, Si XII, emitted at 1-2 MK) were located at the footpoints of a small loop system. These could be interpreted as indirect evidence of chromospheric evaporation. CDS and ground-based observations of an eruptive C2 flare were also reported by Teriaca et al. (2003). Brosius and Phillips (2004) also presented CDS observations of a larger M6 flare. The position of the CDS slit was fixed, thus sacrifying spatial coverage in favour of a high (10s) time resolution. Their observations were consistent with non-thermal particles transferring most of the energy into the chromosphere and creating oppositely-directed flows.

The blue-shifts seen in the emission from high temperature flare plasma are in fact thought to be driven by non-thermal electrons accelerated during the primary energy release (Antonucci et al., 1984) and may occur when the heating rate due to collisions of non-thermal electrons with the ambient plasma in upper layers of the chromosphere exceeds the chromospheric radiative losses (Fisher, 1987). This occurs when the temperature of the heated region is above 2×10^5 K and thus this kind of evaporation cannot be seen in chromospheric spectral lines which are formed in a cooler plasma.

If a region of the chromosphere heated by non-thermal electrons is thick enough, then the rapid temperature increase produces an enhanced pressure in the heated region. This overpressure, besides the evaporation, also drives downward-moving cool and dense *chromospheric condensations* (Fisher et al., 1985) which seem to be responsible for red-shifts of the Hα line profiles reported by many authors (Svestka, 1976, Ichimoto and Kurokawa, 1984).

In this paper we present new CDS observations of the initial phase of the M1 flare of October 22, 2002. We focus primarily on the nature of the blue shifted emission from high temperature plasma and its relationship with the cool chromospheric emission and the hot flare emission. In Sect. 2 we summarise the observing campaign, while in Sect. 3 we present the CDS results in detail, paying particular attention to the measurement of wavelength shifts. In Sect. 4 we discuss the magnetic topology of the flare according to a non linear force free field extrapolation of the magnetic field obtained from THEMIS magnetograms. The flows of the flare plasma are presented and discussed in this context (Sect. 5).

2. Co-ordinated observing campaign for 22nd October 2002

A coordinated observational campaign was organised to follow the evolution of the NOAA 0162 active region during October 22, 2002. Ground based instruments (THEMIS and Vacuum Tower Telescope - VTT - on Tenerife, Canary islands, Spain) and space observatories (SOHO, TRACE and RHESSI) were involved. The active region had several flares, including an M1 flare. RHESSI did not observe the initial phase of the M1 flare. The morphology and evolution of the M1 flare

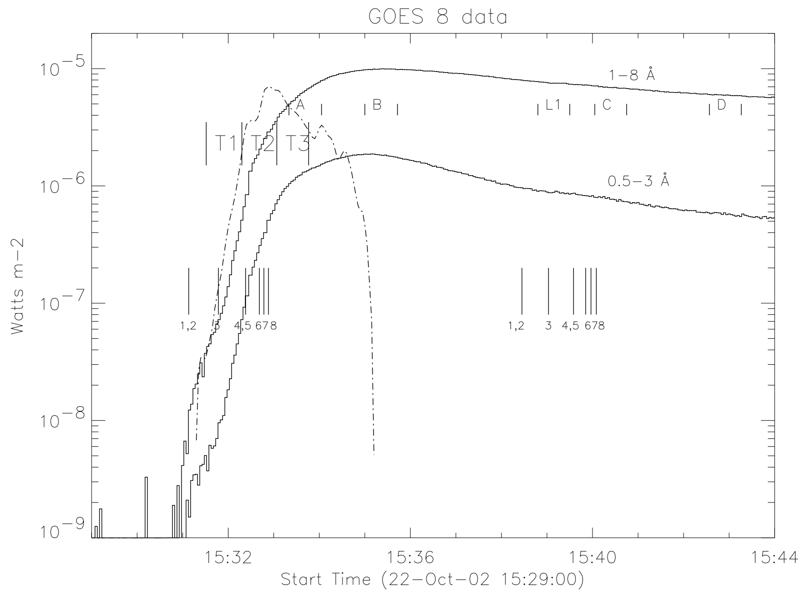

Figure 1. Time evolution of the GOES 8 X-ray fluxes on October 22, 2002 during the M1 flare and the CDS raster scan. The dot-dashed curve is the time derivative of the 0.5–3 Å light curve, and can be used as a proxy for the hard X-ray emission. The timings of a few key observations are indicated (top: CDS slit positions, see Figures 3 and 6; middle: first three TRACE images (T1,T2,T3) in the initial phase of the flare, see Fig. 3; bottom: Hα slit positions during two consecutive VTT/MSDP rasters, see Fig. 9).

during the gradual phase (when RHESSI was observing) were presented in Berlicki et al. (2004) (Paper I).

The active region NOAA 0162 was mainly bipolar, quite extended, and relatively active. The SOHO/CDS sequence of observations was extensive and ran during 08:02-13:07 UT and 15:18-18:13 UT (see Table I). The CDS observations, described in detail below, consisted of rasters during which the slit was scanning the active region.

During October 22 the active region produced at least 3 flares. The main M1 flare occurs at 15:30 UT during the CDS raster at 15:18:16–15:43:16 UT. Fig. 1 shows the X-ray light curves from GOES 8 during the CDS scan. The time derivative of the 0.5–3 Å light curve can be used as a proxy for the hard X-ray emission, and indicates a peak at 15:33 UT. The timings of some CDS slit positions and some TRACE and ground-based observations are also shown.

VTT/MSDP observations in Hα consisted of 9 raster scans between 15:30 and 16:17 UT and a field-of-view of about 380"$\times$170" (exposure time of 0.5s). The rastering was performed from east to west, in the opposite direction compared to CDS. Below we will concentrate on the

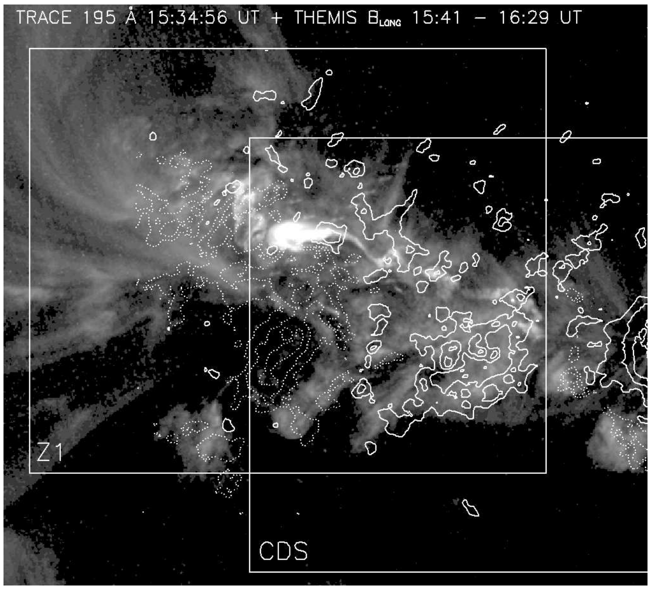

Figure 2. TRACE 195 Å image of the active region during the M1 flare. with contours (± 200, 500, 1000 G) from the THEMIS magnetogram obtained in the Na D1 line. The fields of view of the TRACE sequence of images (Z1, see Fig. 3), of the region of the M1 flare and of the CDS raster are also shown.

Table I. CDS rasters analysed - 22 Oct 2002.

Time (UT)	CDS files	CDS study
8:02:50–8:27:54	s26053r00	SIG_FT44
	s26054r00	ARDIAG_2
	s26054r01	ARDIAG_2
	s26055r00	ARDIAG_2
	s26056r00	SIG_FT44
15:18:16–15:43:16	s26058r00	SIG_FT44
15:43:30–17:07:33	s26059r00	ARDIAG_2
17:08:03–18:32:46	s26059r01	ARDIAG_2

first VTT spectral raster, which scanned the active region during 15:30-15:37 UT, i.e. in the impulsive phase. Results from the follow-up raster (gradual phase) have been presented by Berlicki et al. (2005) (Paper II).

TRACE 195 Å images were obtained at high-cadence (40 s) between 15:29 and 15:41 UT (with a FOV 384”×384” and a 1” resolution)(see

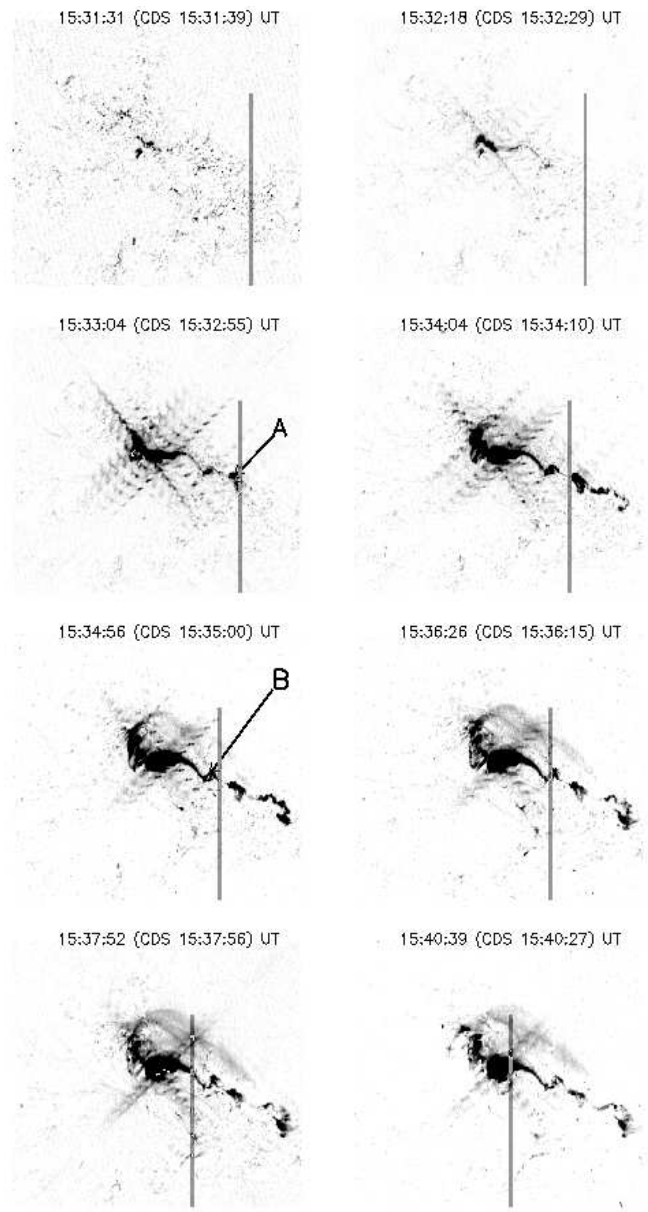

Figure 3. Sequence of TRACE 195 Å difference images (negative) of the region Z1 (cf. Fig. 2) and centred during the peak of the M1 flare. The image that has been subtracted was taken at 15:29:59 UT, before the start of the flare. The timings indicate the initial exposure time for each TRACE image, and the corresponding nearest CDS exposure. The location of the CDS slit is also shown.

Fig. 2 for the full TRACE FOV). Before and after this time the TRACE observations were obtained with slightly lower time resolution (50 s) and larger FOV (512"×512"). Fig. 3 shows a sequence of TRACE 195 Å difference images in the central part of the TRACE FOV, where the flare took place. The location and timings of the CDS slit are also indicated in Fig. 3. The first obvious signature in the TRACE 195 Å occurs at 15:32:18 UT (T2, see Fig. 1), somewhat later than the increase in the GOES X-ray flux. However, a small brightening already appears at the same location on the 15:31:31 UT TRACE image (T1, see Fig. 1). By 15:33 UT (T3, see Fig. 1), the entire ribbon structures (located on either side of the neutral line) brighten up in the TRACE 195 Å image. The Hα ribbons were already visible at 15:31 UT (see Paper I and Figure 9).

After this intial phase, a system of high-lying and expanding loops starts to appear as a weak feature in the in TRACE 195 Å images (See Figures 3 and 5). CDS had the slit positioned over the main area of the flare during the peak and gradual phase (cf. Fig. 1 and Fig. 3) and can therefore be used to estimate the temperatures of the various features recorded by TRACE. As shown below, CDS observed strong Fe XIX emission in the locations of both the ribbons and the higher-lying loops observed by TRACE, which suggests that most likely the TRACE 195 Å images are dominated by hot emission from Fe XXIV.

3. CDS instrument and data analysis

The CDS observations were performed with the normal incidence spectrometer (NIS). The internal scan mirror allows CDS to scan with the long slit an area of $4'$ square within a single 'raster', from west to east. The CDS observing sequences were specifically designed to study compact flares, and included a range of spectral lines, in particular the high-temperature Fe XIX 592.2 Å. CDS observed NOAA 0162 with two types of rasters (see Table I): 1) a slow diagnostic raster (1hour 20 m, CDS study name ARDIAG_2) that extracts many diagnostic lines; 2) a fast raster (slit exposure of 18s for a total duration of 20 m, CDS study name SIG_FT44) that only extracts a few lines, selected to cover a wide range of temperatures (see Table III).

One important aspect of CDS is that lines emitted from the chromosphere up to the corona are observed. This is very useful for a proper co-alignment with other datasets, e.g. photospheric magnetic fields from SOHO/MDI, and coronal images from TRACE. The NIS data were processed using the standard corrections. Line-fitting techniques have been used to determine the moments of each of the spectral lines

Table II. List of the main lines used for the wavelength calibration. The first row gives the reference wavelengths (λ_{st}, Å) adopted. The second row gives the wavelengths (λ_1, Å) as obtained from the pre-flare raster s26055 and the calibration curve adopted. The third row gives the corresponding relative velocities (v_1, km/s). The following two rows give wavelengths (λ_2, Å) and relative velocities (v_2, km/s) as obtained from the post-flare raster s26059 and using the same calibration curve. Note the small differences in the measured wavelengths, giving confidence in the stability of the wavelength calibration.

	Si XII	He I	Ne IV	Al XI	O IV	O IV
λ_{st}	520.665	522.210	542.07	550.06	553.34	555.263
λ_1	520.675	522.208	542.031	550.070	553.365	555.252
v_1	5	-1	-21	5	13	-6
λ_2	520.664	522.211	542.061	550.066	553.354	555.260
v_2	0	0	-4	3	7	-1
	Ca X	Ne VI	Ne VI	Fe XII	Mg X	O V
λ_{st}	557.765	558.594	562.803	592.60	624.941	629.732
λ_1	557.758	558.590	562.791	592.590	624.936	629.735
v_1	-3	-2	-6	-5	-2	1
λ_2	557.769	558.622	562.812	592.597	624.932	629.747
v_2	1	15	5	-1	-4	6

by removing the scattered light component. In SOHO post-recovery spectra the NIS line profiles are no longer gaussians, and show a broadened and asymmetrical long wavelength wing, which is approximately constant and can therefore be accounted for. Significant line broadening can still be measured. The CDS radiometric calibration of Del Zanna et al. (2001) has been adopted here, with a correction to take into account the effects on the NIS detector of the gain depression caused by exposures with the wide slit.

3.1. Wavelength calibration

In order to deduce velocities, it is necessary to have an accurate wavelength calibration for the CDS spectra. CDS does not have an absolute wavelength calibration, nor does it have any photospheric or chromospheric lines (except He I) which could be used as wavelength references. This means that the CDS wavelength calibration has to be carried out using the observed transition region and coronal lines for each set of observations. Changes in CDS wavelength calibration have

Table III. Some of the prominent lines in the CDS/NIS wavelength bands, used in this paper. Wavelengths are taken from the CHIANTI database unless otherwise stated. Those indicated with an asterisk have been used for the wavelength calibration. When only one decimal place is indicated, the lines are blends of at least two transitions. The approximate temperature of maximum ion abundance (in ionization equilibrium) is also indicated, together with the channel and the CDS study that recorded the lines (FR: fast raster; DR: diagnostic raster, see text).

Ion	wavelength (Å)	log T_e	NIS	
Si X	347.402	6.1	1	FR,DR
Si X	356.0	6.1	1	FR,DR
Si XII	520.665*	6.3	2	FR,DR
He I	522.210*	4.5	2	FR,DR
O IV	553.34*	5.3	2	FR,DR
O IV	554.076	5.3	2	FR,DR
O IV	554.513	5.3	2	FR,DR
O IV	555.263*	5.3	2	FR,DR
Fe XIX	592.16	6.9	2	FR,DR
Fe XII	592.60*	6.1	2	FR,DR
Mg X	624.941*	6.0	2	FR,DR
O IV	625.853	5.3	2	FR,DR
O V	629.732*	5.4	2	FR,DR

been observed (up to 0.1 Å in NIS 2) due to temperature changes in the CDS instrument (C.D.Pike, priv. comm.), in particular when moving from disk to off limb and visa-versa.

For the wavelength calibration, it is important to have accurate 'standard' rest wavelengths. We have adopted the values shown in Table III, mainly from the CHIANTI database (v 4.2) which in turn incorporates most values from NIST. Special care has been taken to assertain an accurate rest wavelength value for the Fe XIX 592.2 Å line. Our calibration gives a value of 592.16 Å, consistent with the careful flare studies of Skylab NRL spectroheliogram data by Widing (1978), but different from other work (e.g. Sandlin et al. (1976) who reported a value of 592.24 Å and Lawson and Peacock (1980) who's laboratory work implied a value of 592.522 Å). An extra complication in the line profile fitting for the Fe XIX line is the presence of a line

(Del Zanna et al., 2002a), recently identified with an Fe XII transition at 592.6 Å(Del Zanna and Mason, 2005).

To calibrate the CDS observations, average CDS spectra containing a large number of lines (the diagnostic rasters) of two rasters taken before and after the flare have been analysed and wavelength-calibrated. We assumed for the CDS pixel-wavelength calibration a quadratic function. The wavelength calibration was remarkably stable over the period of the observations. Table II shows that in most cases the line centres were within a few km/s the assumed reference values.

In terms of uncertainties, we note that the positions of the line centres can be calculated to approximately 0.1 Å, which is equivalent to about 10 km/s. There may be some other systematic uncertainties (for example due to geometrical distortions within CDS) but these are difficult to quantify. We note that spectral resolution of CDS does not easily allow a stationary and shifted component to be resolved simultaneously. Hence, our results refer to the average displacement of each line profile. We note that Fe XIX is only present during flares, and that otherwise the Fe XII line dominates.

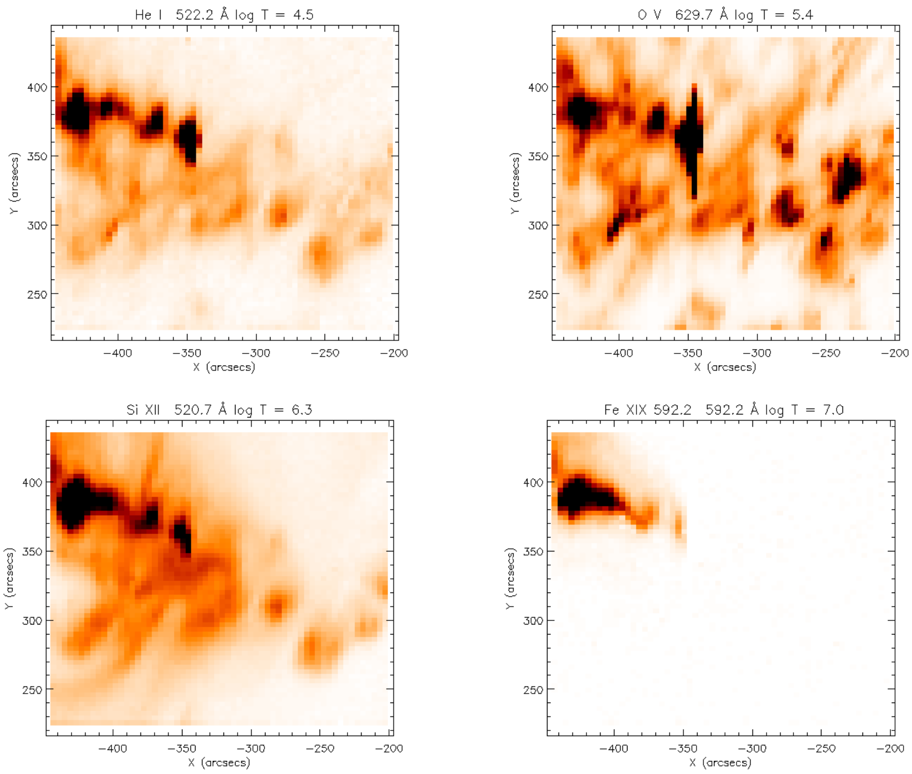

Figure 4. Monochromatic images (negative) obtained from the CDS raster.

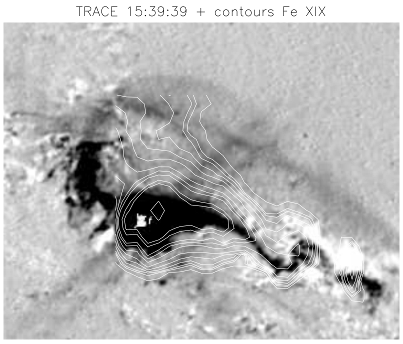

Figure 5. TRACE 195 Å difference (negative) image with contours of Fe XIX intensity. Note the bright emission, cospatial with the ribbon and the Fe XIX intensity. Also note the weaker high-lying loops connecting the two ribbons.

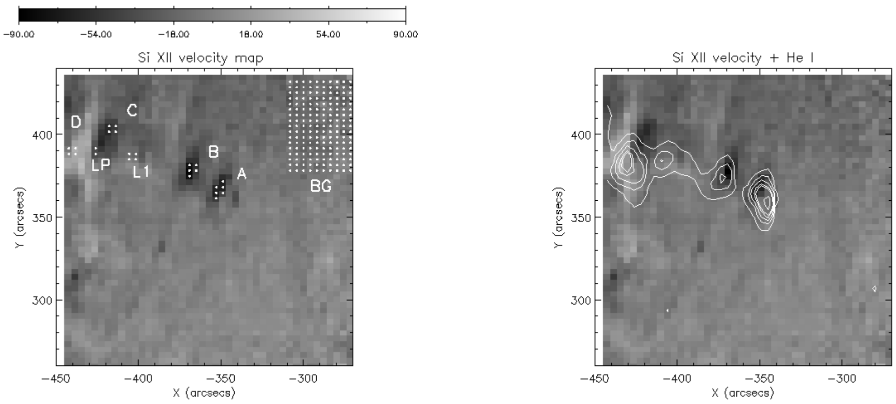

Figure 6. Si XII 520.665 Å velocity map in the flare region, with the areas selected for further analysis. Areas A,B,C correspond to regions of strong blue-shifts, while area D of red-shift. Region LP corresponds to the area of peak Fe XIX 592.16 Å intensity, while region L1 is where the central part of the flare loop is located. Region BG is a 'background' reference region. The left image shows the Si XII 520.665 Å map with contours of the He I intensities.

3.2. Overview of the CDS results

Fig. 4 shows monochromatic images obtained from the CDS raster, in lines emitted over a broad temperature range. The ribbon structure is so bright in He I and also at transition region temperatures (e.g. O V) that the brightest lines saturated the detector in some positions (region

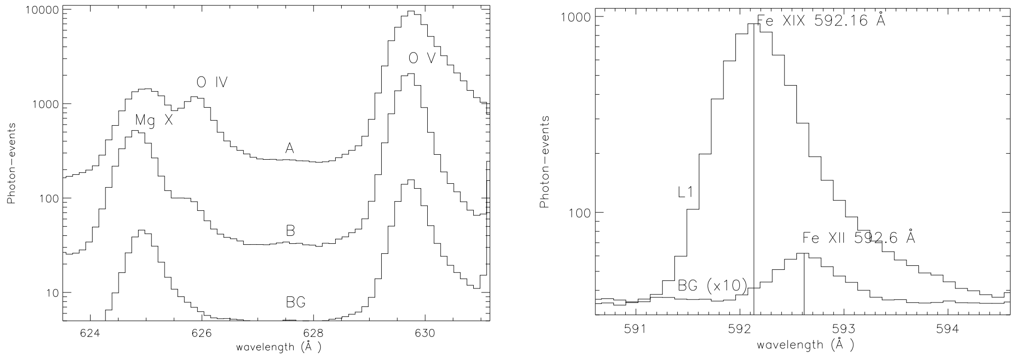

Figure 7. Left: Spectra of three different regions, A,B,BG. Note that in region A the profiles of the strongest lines are nearly saturated. The O IV line has been used for density measurements at transition-region temperatures. Right: Spectra of the region L1 (peak flare), and of the background BG (multiplied by ten), showing the Fe XIX 592.16 Å and the previously unidentified Fe XII line. Outside of the flaring region, all the intensity is due to Fe XII.

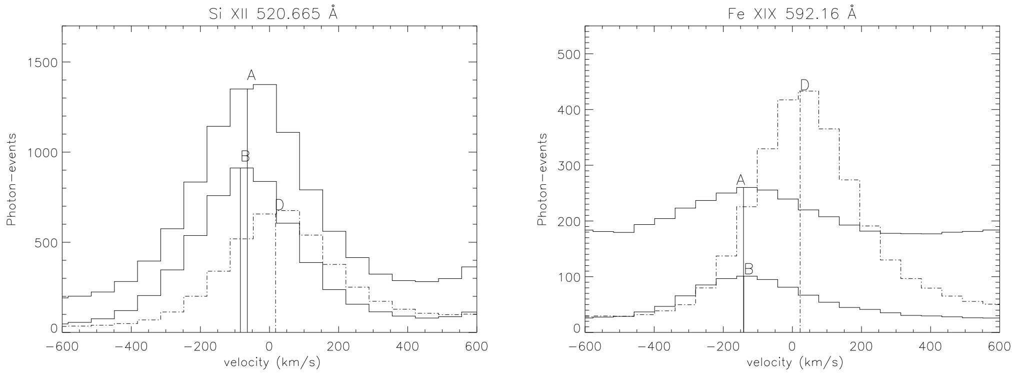

Figure 8. Line profiles in regions A,B,D showing the evident blue-shifts in the coronal (Si XII) and flare (Fe XIX) lines in regions A,B.

A, defined below). The hot emission from Fe XIX is only present in the ribbon and high-lying loop structures seen in the TRACE 195 Å band (see Fig. 5).

The velocity maps show a consistent pattern. Large velocities, mainly upflows, are only visible in lines formed above 1 MK, and in the Fe XIX flare line. Fig. 6 shows as an example a velocity map in the flare area obtained from a Si XII line, and the regions selected for further study. Line fitting was performed on the averaged spectra of these selected regions. Figs. 7,8 show some line profiles in a few selected regions. Table IV presents some results of the line fitting, in particular velocities, intensities and line widths. Line velocities are also plotted in Fig. 11.

Regions A,B were associated with the brightest emission in the chromospheric-TR lines, and with strong upflows in the Fe XIX flare line. Region A was observed by CDS during 15:33:20–15:34:10 UT (see Fig. 3 for the correspondence with TRACE), i.e. in the impulsive phase of the flare (Fig. 1). Region B was observed during 15:35:00–15:35:50 UT, i.e. at the time of the peak X-ray emission (Fig. 1). The blueshifts in region B show an exponential behaviour with increasing temperature of line formation. They are 27 km/s in He I, 60 – 88 km/s in Mg X, Si XII, and 140 km/s in Fe XIX. Region A shows a similar behaviour but with a slight downflow in the cooler line (He I). The downflows in O IV and Mg X are questionable because of detector saturation. As observed in other cases (Del Zanna et al., 2002b), upflows are seen in both Si XII and Mg X lines. We note that in contrast to our results, Brosius and Phillips (2004) found conflicting line shifts in these lines, thus discouraging the use of the Mg X 625 Å line because of blending with O IV.

In terms of line widths, aside from a few notable exceptions, the full-width at half maximum ($FWHM$) values are close to the value of the instrumental width (0.5 Å in post-recovery spectra). The exceptions are in regions A,B,D and mostly in the coronal lines. Interestingly, the Fe XIX line has a large width in all of the regions, suggestive of large turbulent motions. As also noted by Brosius and Phillips (2004), the observed blue-shifts are not superimposed on a stationary component, but appear as shifts of the entire line profiles in Mg X, Si XII and Fe XIX (see Fig.8).

The other regions were close to the flare site. Region L1 shows near-zero line-of-sight velocities in all lines. The region LP corresponds to the area of peak X-ray emission, as judged from the TRACE 195 Å images and the Fe XIX emission, observed by CDS 7 minutes later, around 15:42 UT. It is interesting to notice that, on the opposite sides of the peak emission, flows of opposite directions are observed (region C, upflow; region D, downflow) in all the lines, emitted from TR to flare temperatures.

Region BG was chosen as a background reference region, not involved in the flare. The lines show near-zero line-of-sight velocities. Note that the intensity of the Fe XIX line is an upper limit (the emission being dominated by the Fe XII 592.6 Å). We have compared the line intensities of the background region with other observations of the quiet Sun, and found that, for the transition region lines, the values are very close to those of the average quiet Sun.

The O IV lines (cf. Fig. 7) are an useful density diagnostic at transition region temperatures, and in the locations of strong brightenings.

Table IV. Results from the averaged spectra of the various regions displayed in Fig. 6. For each of the selected spectral lines, we display the averaged velocities v (in km/s; negative corresponds to blue-shift), the calibrated line intensities I (erg cm^{-2} s^{-1} sr^{-1}), and the full-width at half maximum $FWHM$ (Å). O IV(a) indicates the 553.4 Å line, while O IV(b) indicates the 625.8 Å line, used to obtain the electron densities N_e (cm^{-3}). Large blue-shifts are mostly observed in regions A,B,C. Note, however, that some of the lines are close to saturation in region A, and values are uncertain (they are indicated in parentheses).

Region	A	B	C	D	L1	LP	BG
He I v	13	-27	-30	-17	-17	-36	-22
I	2393	770	112	377	751	1293	16
$FWHM$	0.61	0.53	0.51	0.56	0.51	0.51	0.50
O IV(a) v	(33)	-21	-24	13	0	-20	0
I	(9818)	598	80	237	252	686	33
O IV(b) I	2333	111	-	-	-	-	-
N_e (O IV)	2 10^{11}	0.9 10^{11}	-	-	-	-	-
O V v	(23)	-25	-21	0	-12	-28	-4
I	(33226)	5038	721	2490	2840	6782	387
$FWHM$	(0.70)	0.50	0.50	0.55	0.50	0.50	0.50
Mg X v	(14)	-62	-51	29	-17	-37	-5
I	(5910)	1630	656	1205	1781	17093	118
$FWHM$	(0.80)	0.59	0.53	0.58	0.58	0.52	0.52
Si XII v	-64	-84	-54	17	-6	-40	-10
I	2756	1847	839	1378	2818	16748	63
$FWHM$	0.59	0.55	0.50	0.55	0.51	0.50	0.50
Fe XIX v	-141	-140	-56	22	-13	-26	-
I	294	272	694	1271	2721	7544	≤ 0.5
$FWHM$	0.68	0.65	0.56	0.59	0.57	0.55	-

For both the upflow regions A and B we obtain averaged line-of sight electron densities of $\simeq 10^{11}$ cm^{-3}.

4. Magnetic topology and Hα ribbons

For the analysis of the Hα Dopplershifts we used the observations of VTT/MSDP obtained at 15:30-15:36 UT and followed the methods described in Paper II. We selected areas (Fig. 9) corresponding to the regions observed by SOHO/CDS. These regions were not observed at the same time as CDS because of the opposite direction of the scanning of these two instruments. The profiles in areas 1 and 2 (east ribbon) are observed close to the onset of the flare. They are very flat or asymmetric and cannot be fitted because they cover a rather small wavelength range (± 0.6Å). Nevertheless, the shape of the profiles is consistent with strong downflows (30-40 km/s).

Regions 6,7,8 in the west ribbon correspond to region A in the CDS spectra; 4,5 to region B; and 3 to region L1. For those regions (3-8) we have obtained very similar values as those obtained in the successive raster (Paper II), i.e. smaller upflows in regions 4,5 (3 km/s) and higher upflows (7 km/s) in regions 6,7,8.

In Paper I we presented the magnetic topology of the active region. The magnetic field shows that this active region was highly sheared. The trigger of the flare was the emergence of a locally very twisted magnetic flux (bipole). The linear force-free-field extrapolation of the magnetic field lines obtained from the THEMIS magnetogram (cf. Figure 10) provides an explanation of the asymmetry of the east (1,2) and west (3-8) ribbons and of the fast propagation of the brightening along the west ribbon (of the order of a few min) from the emerging bipole towards the leading spot. This propagation can be explained by the reconnection of the growing emerging field lines with the higher and higher overlying magnetic field.

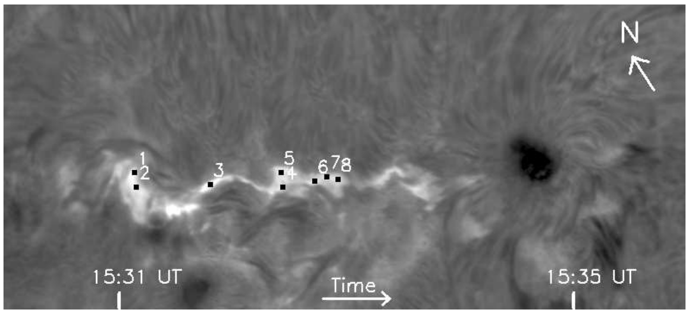

Figure 9. VTT/MSDP image of AR 0162 taken between 15:30 and 15:36 UT with dots which mark the areas where the Hα line profiles were obtained. The timing and scanning direction are also indicated.

5. Discussion and conclusions

We have presented multi-wavelength observations of a compact M1 flare, mainly with CDS, TRACE, VTT/MSDP and THEMIS. In two earlier papers (Paper I and II) we discussed the gradual phase. In this paper, we concentrate mainly on SOHO/CDS flow analysis during the

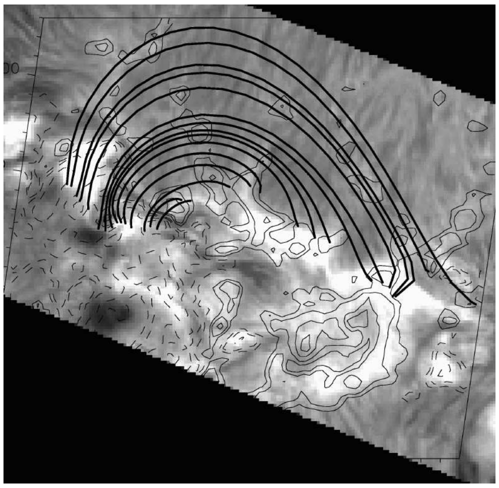

Figure 10. Extrapolated field lines over the active region explaining the fast propagation of the brightening of the flare ribbon by the rise of the emerging flux, in the plane is represented the photospheric longitudinal magnetic field observed with THEMIS in the Na D1 line

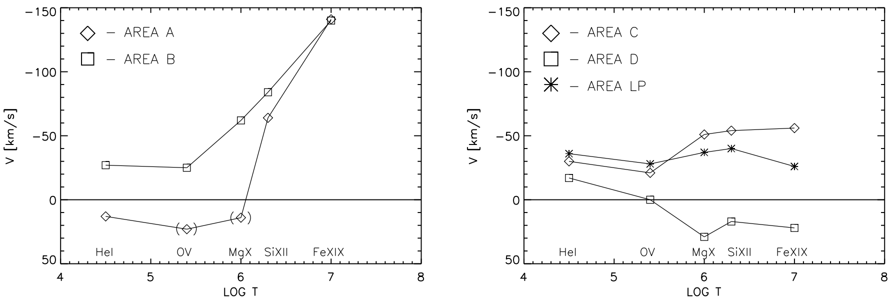

Figure 11. Flows observed in flare kernels over a large temperature range for different CDS lines: strong blue-shifts in regions A and B for hot lines, weak blueshifts in regions C,and LP, slight redshifts in region D. The error bar is +/- 10 km/s. The measurements in parentheses are uncertain due to saturation of the CDS detector.

initial phase. With CDS we could make some accurate measurements of velocities over a range of temperatures (10^4 K to $8 \cdot 10^6$ K), for which we have proposed an explanation.

As seen in the X-rays (GOES), the flare started at 15:31 UT and reached peak emission in just 3 minutes. Soon after the peak X-ray emission, long-lasting chromospheric (Hα) ribbons form across the neutral line. Strong TRACE 195 Å emission, cospatial with Hα also forms as a brightening along the ribbons. The simultaneous CDS observations show that the hot (8 MK) Fe XIX emission is cospatial with TRACE

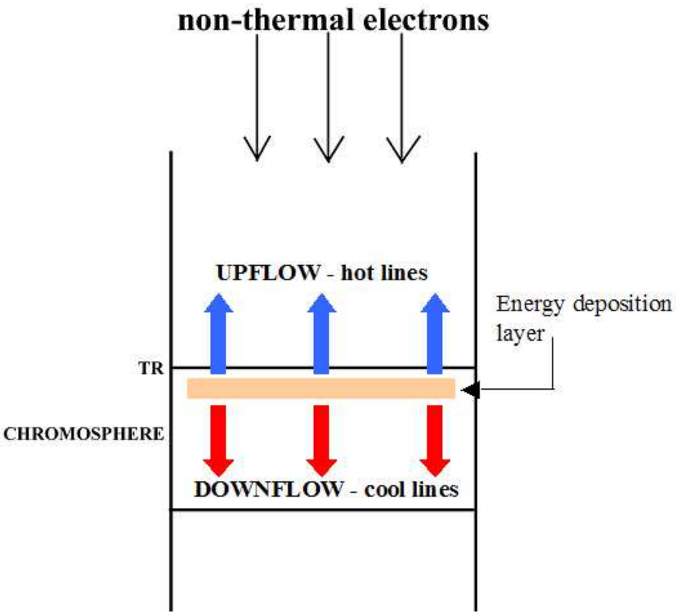

Figure 12. Sketch of the precipitation of the electrons from the site of reconnection towards the low atmosphere and the expected flows according the temperature of formation of the observed lines.

195 Å, and we can therefore propose that the bulk of the TRACE emission is due to the Fe XXIV 192.0 Å(12 MK) flare line.

It is a rare opportunity to observe with CDS during the initial (peak) phase of a flare (15:33-15:36 UT). We find upflows concentrated in small spatial areas in the ribbon (in regions A,B, 15:33-15:36 UT). The blueshifts in region B show an exponential increase with temperature of line formation (27 km/s in He I, 60 – 88 km/s in Mg X, Si XII, and 140 km/s in Fe XIX). Region A shows a similar pattern, with a possible downflow in the cooler lines (Figure 11).

We stress the fact that the observed upflows correspond to full shifts of the line profiles, in regions where the coronal/flare line intensities are relatively weak. Instruments (such as the above-mentioned BCS or FCS) without the CDS spatial resolution would have not been able to observe these localised blue-shifts. The large line-widths in the Fe XIX line indicate the existence, in the upflow regions, of strong turbulent velocities at high temperatures, in addition to the overall flows.

In both A,B regions the cooler transition region lines show concentrated brightenings with intensities increased by factors of $\simeq$300, 20. We were able to use the CDS O IV line ratios to measure electron densities of the order of 10^{11} cm^{-3} for the regions A,B, i.e. a factor of 10 higher than the quiet Sun values (cf. Del Zanna and Bromage, 1999). These are somewhat lower that the values of 10^{12} cm^{-3} derived from the Hα data (Paper II). Such measurements of densities and velocities at different temperatures should give important constraints to the modelling of the atmosphere above the ribbons.

Based on the above measurements, we interpret the upflows observed in regions A and B (Fig. 11) as due to chromospheric evaporation. We suggest that the upflows observed in hot lines in A and B correspond to the so called "explosive evaporation" and the small downflow observed in He I (area A) is due to the overpressure of the chromosphere. These regions are relatively far from the flare onset site (location of a small emerging bipole) but they became bright 2-3 minutes after the onset of the flare. This rapid propagation could be explained by a chain of reaction of successive reconnections in the high corona as the emerging flux field lines reconnected with higher and higher preexisting magnetic field. This is confirmed by a linear force-free analysis of the magnetic topology.

Non-thermal electrons are probably responsible for the high flows in the ribbons (Fig. 12). A system of high-lying and expanding loops in TRACE 195 Å forms subsequently (Figure 5). Cospatial CDS observations in Fe XIX suggest that these are high-temperature loops and could be associated with the reconnecting loops.

The areas C, D, LP in the ribbon were observed by CDS ten minutes after the onset of the flare, and do not exhibit strong flows. Areas C and and LP exhibited upflows between -30 to -55 km/s according to the temperature of formation of lines with a slight increase versus temperature. This evaporation could be driven by the large conductive heat flux from the flare plasma contained in the high-temperature loops. The small downflows observed in point D are ambiguous and difficult to be explained in this context.

The Hα ribbons were not observed with VTT/MSDP simultaneously with CDS even if their observations times were overlapping (cf. Fig.1). The scanning of both instruments were done in opposite directions thus the kernels are not reached at the same time. Therefore it is difficult to have a direct comparison. The asymmetry of the Hα line profiles in points 1 and 2 suggests strong redshifts of the chromospheric plasma. These profiles were observed at 15:31 UT. This time corresponds to the increase of the GOES soft X-ray flux and this redshift could correspond to the flow that is expected for cool plasma during the impulsive phase. The Hα line profiles in points 5, 6, 7,8 are similar to those analysed by Paper II during a later phase of this flare. The Doppler-shifts derived from the profiles of Hα using a non-LTE radiative transfer code with a flare model correspond to small upflows (2 to 10 km/s, Paper II) and could correspond to the "gentle evaporation" observed during the subsequent gradual phase of the flare.

Our observing campaign and analysis emphasises the importance of combining multi-wavelength observations in order to understand the dynamics of a solar flare. It is also essential to use spectroscopic observations to obtain an unambiguous determination of the plasma properties, in particular flows. Spatially-resolved observations are also fundamental to establish the locations of the flows, to relate them to the hot flare emission.

Other authors (e.g. Brosius and Phillips, 2004) have adopted a different observing approach, i.e. to fix the slit position and rely on the imaging instruments to study the morphology of an event. Flows at the slit position persisted on time-scales of minutes after the onset of the flare. Upflows ($\simeq$60 km/s) in flare lines and downflows ($\simeq$40 km/s) in cooler transition region lines were observed during the impulsive phase. However, a fixed position of the CDS slit makes it impossible to study the 2D behaviour of the flows within the flare.

Neither the scanning approach or the sit-and-stare approach is however entirely satisfactory. We look to future projects, such as SOLAR-B, which will enable us to study active regions and flares in much more detail through all layers of the solar atmosphere.

Acknowledgements

GDZ and HEM acknowledge support from PPARC.

This research was partially supported by the European Commission through the RTN programme ESMN (European Solar Magnetism Network, contract HPRN-CT-2002-00313). AB and BS are members of ESMN. SOHO is a project of international collaboration between ESA and NASA. These observations were performed during a MEDOC campaign (JOP 157). The magnetic field extrapolations were obtained from the code FROMAGE (FRench Online MAGnetic Extrapolations) We acknowledge the use of the SURF, TRACE, SOHO on-line databases.

References

Antonucci, E., A. H. Gabriel, L. W. Acton, J. W. Leibacher, J. L. Culhane, C. G. Rapley, J. G. Doyle, M. E. Machado, and L. E. Orwig: 1982, *Sol. Phys.* **78**, 107–123.

Antonucci, E., A. H. Gabriel, and B. R. Dennis: 1984, *ApJ* **287**, 917–925.

Bentley, R. D., G. A. Doschek, G. M. Simnett, M. L. Rilee, J. T. Mariska, J. L. Culhane, T. Kosugi, and T. Watanabe: 1994, *ApJ* **421**, L55–L58.

Berlicki, A., B. Schmieder, N. Vilmer, G. Aulanier, and G. Del Zanna (Paper I) : 2004, *A&A* **423**, 1119–1131.
Berlicki, A., P. Heinzel, B. Schmieder, P. Mein, and N. Mein (Paper II): 2005, *A&A* **430**, 679.
Brosius, J. W. and K. J. H. Phillips: 2004, *ApJ* **613**, 580–591.
Czaykowska, A., B. de Pontieu, D. Alexander, and G. Rank: 1999, *ApJ* **521**, L75–L78.
Del Zanna, G. and B. J. I. Bromage: 1999, *J. Geophys. Res.* **104**, 9753–9766.
Del Zanna, G., B. J. I. Bromage, E. Landi, and M. Landini: 2001, *A&A* **379**, 708–734.
Del Zanna, G., S. E. Gibson, H. E. Mason, C. D. Pike, and C. H. Mandrini: 2002a, *Advances in Space Research* **30**, 551–556.
Del Zanna, G. and H. E. Mason: 2005, *A&A* **433**, 731.
Del Zanna, G., H. E. Mason, and C. Foley: 2002b, *ESA SP-506*, pp. 585–588.
Doschek, G. A., R. W. Kreplin, and U. Feldman: 1979, *ApJ* **233**, L157–L160.
Fisher, G. H.: 1987, *ApJ* **317**, 502–513.
Fisher, G. H., R. C. Canfield, and A. N. McClymont: 1985, *ApJ* **289**, 434.
Ichimoto, K. and H. Kurokawa: 1984, *Sol. Phys.* **93**, 105–121.
Lawson, K. D. and N. J. Peacock: 1980, *J Phys B Atomic Molecular Physics* **13**, 3313–3334.
Mason, H. E., R. A. Shine, J. B. Gurman, and R. A. Harrison: 1986, *ApJ* **309**, 435–448.
Sandlin, G. D., G. E. Brueckner, V. E. Scherrer, and R. Tousey: 1976, *ApJ* **205**, L47–L50.
Svestka, Z.: 1976, *Geophysics and Astrophysics Monographs* **8**.
Teriaca, L., A. Falchi, G. Cauzzi, R. Falciani, L. A. Smaldone, and V. Andretta: 2003, *ApJ* **588**, 596–605.
Warren, H. P. and G. A. Doschek: 2005, *ApJ* **618**, L157–L160.
Widing, K. G.: 1978, *ApJ* **222**, 735–739.
Zarro, D. M., G. L. Slater, and S. L. Freeland: 1988, *ApJ* **333**, L99–L101.